Physico-chemical Studies on Surface Active Agents. (V)

The Precipitation of Anionic Surface Active Agents by Metal Ions

Akira WATANABE*

(Tachi Laboratory)

Received March 15, 1960

The reaction kinetics for the precipitation of anionic surface active agents by inorganic ions have been studied by measuring the turbidity change. The process was essentially a sol formation of the surface active agent salts formed; coagulation and sensitisation occurred over certain range of the added electrolyte concentrations. It was demonstrated by means of the electrophoretic mobility measurements that the coagulation occurred either due to decrease in the ζ potential of the sol formed or to the increase in ionic strength. Values of the solubility and solubility product of these surface active agent salts were calculated from the turbidity *vs.* log electrolyte concentration curves. The values obtained were in good agreement with the coagulation concentrations of the corresponding cations for the protected sols described in Part 3. In some cases, especially for alkyl phosphate, optical density *vs.* time curves showed two steps. It was proved by electron microscopy that the first step was the crystal formation and the second the flocculation process.

I. INTRODUCTION

It was demonstrated in Part 3[1] that the coagulation of silver iodide sols, protected with anionic surface active agents, by addition of electrolytes, was intimately related to the strength of binding of the counter ion to the head group of the surface active agent; thus a relationship to the solubility of the salts consisting of the counter ions and the surface active anions would be expected. It is the main purpose of this paper to describe the experimental work which has been carried out in order to establish this relationship and to determine the solubilities of these salts.

The change in turbidity as a function of time after adding the electrolyte solution to the anionic surface active agent solution gives for insoluble salts a useful method for determining the solubility of the surface active agent salt formed. This type of technique has largely been used by Težak and his co-workers[2,3] in studies on the coagulation of inorganic sols in *nascent* state.

It is important to notice that the reaction under some conditions is essentially a formation of a sol of the metal salt of the surface active agent; hence coagulation can be also observed, depending on the initial concentration ratio of the reactants. Coagulation may occur because of high ionic strength (see Part 3) or low surface potential of the sol particles formed (counter ion binding). As has been shown in Part 3 electrophoretic measurements can be used to decide which mechanism is playing the major part in this process.

Very few studies appear to have been made on metal salts of surface active

* 渡 辺 昌

agents[4,5]. However, this work is very important in view of the practical applications of surface active agents, *e. g.* in the separation of minerals by froth flotation[6,7]. As the nature of the bond between the mineral surface and the surface active agent is one of the most important factors in this process, the present work will probably give useful information in clarifying the mechanism and help in deciding which surface active agents should be the most effective for separating the minerals of a particular metal. Free metal ions in solution (depending on the solubility product of mineral) can cause precipitation of surface active agents.

Finally, the salts have been examined by electron microscopy. The micrographs showed interesting crystal shapes and coagula, and gave useful information on the processes of crystal growth and coagulation.

II. EXPERIMENTAL

1. Materials

The anionic surface active agents used were STS, SDBSO and DHP, and the inorganic electrolytes used were the same as those described in Part 3[1].

2. Methods of Measurements

(i) Turbidity

Aliquots of electrolyte solutions in the mixer were added to 3 ml of the surface active agent solution in the optical cell. The turbidity change with time was followed by the same method as described in Part 2[8]. The surface active agent concentrations employed were $10^{-3}\,M$ for STS, $9\times10^{-4}\,M$ for SDBSO and $2.5\times10^{-4}\,M$ for DHP; these concentrations were maintained constant and only the metal solution varied.

(ii) Microelectrophoresis

After the turbidity measurement the sol formed in the optical cell was transferred to the microelectrophoresis cell and the mobility of the particles determined, see Part 2[8].

Under certain conditions, especially at high concentrations of electrolytes, various shapes of crystals were observed, *e. g.* rods and plates. Particles appearing to have more or less spherical shapes were chosen for measurements of mobility in order to avoid the influence of shape factor on the mobility reading as much as possible[9].

(iii) Electron Micrographs

These were obtained in the manner previously described[8]. Direct deposition of samples on to nitrocellulose film was employed.

III. RESULTS

1. Turbidity Behaviour

(i) Optical Density *vs.* Time Curves

Although the original purpose of these measurements was the determination of the solubility products of the metallic salts of the surface active anions, it was found

that the turbidity changes with time showed very interesting behaviour.

Some of the typical turbidity *vs.* time curves are given in Fig. 1, 2 and 3, for

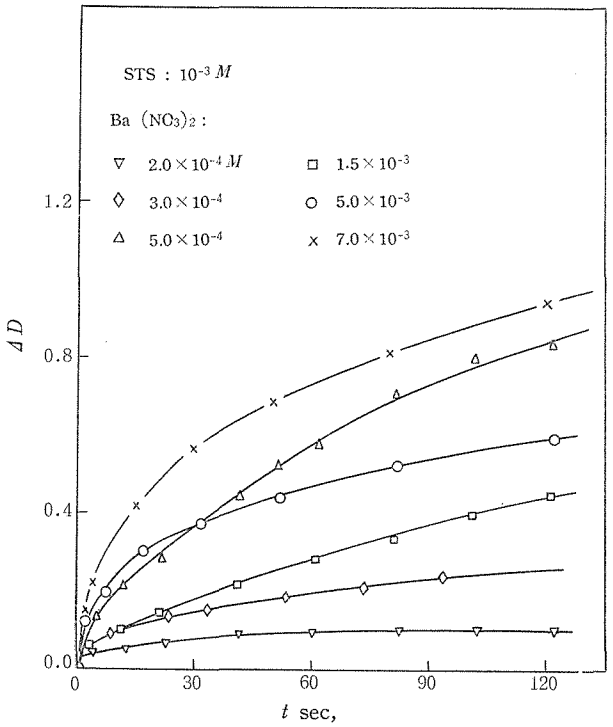

Fig. 1. Δ Optical density *vs.* time for formation of barium tetradecyl sulphate.

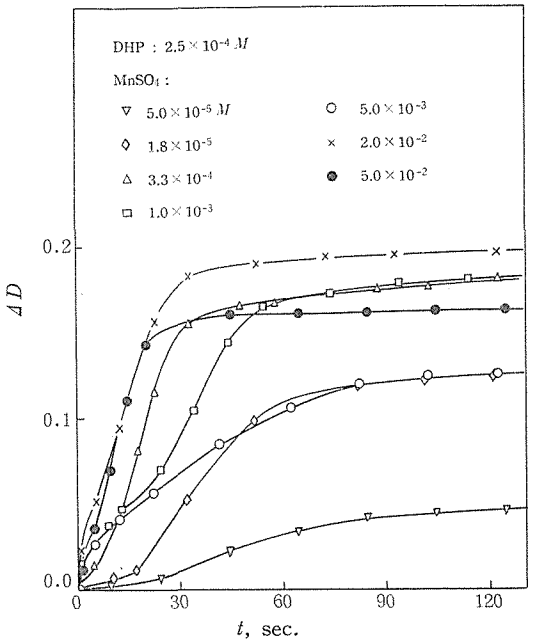

Fig. 2. Δ Optical density *vs.* time for formation of manganese dodecyl phosphate.

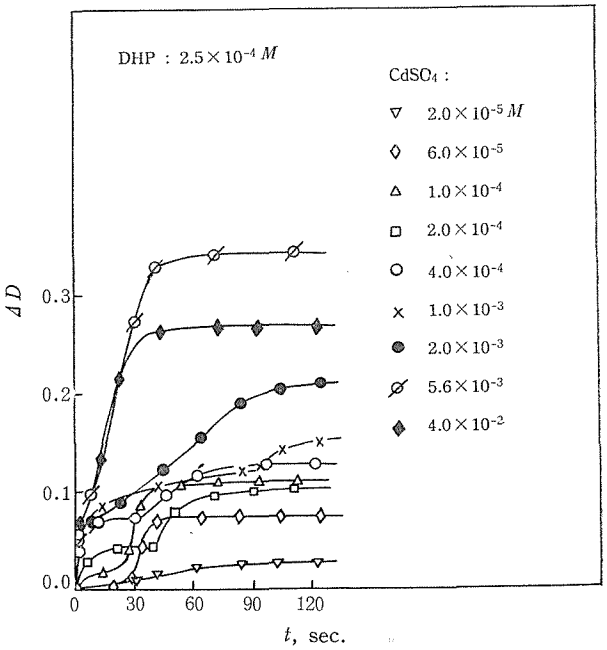

Fig. 3. Δ Optical density *vs.* time for formation of cadmium dodecyl phosphate.

reactions between barium and tetradecyl sulphate ion (TS^-), manganese and dodecyl hydrogen phosphate ion (DP^-) and cadmium and DP^- ions; in the case of DHP, the *p*H of the surface active agent solution was *ca.* 4.5 and therefore the compound was mainly in the singly ionized form[10], see Part 2[8].

The curves show various types of behaviour depending on the concentrations of the surface active anions and cations employed; moreover, even for the same combination, marked differences were observed at different concentration ranges of electrolyte. In some cases the normal types of curve, as obtained in the formation of silver iodide sols in the presence of surface active agents (see Part 6)[11] were observed, *e. g.* in the reaction between barium and TS^- ions, see Discussion.

(ii) Optical Density at Different Times

The optical densities at 30, 60, 90 and 120 sec after mixing are plotted against the logarithm of molar concentrations of the electrolyte in Fig. 4, for the reaction between lanthanum and $DBSO^-$ ions. It is found that extrapolation of the steepest portion of the left hand side of each curve leads to intersection on the log c_e axis at the same point. The convergence obtained with the present reactions was usually poorer than that obtained with the systems described in Parts 2 and 6. However, reasonable values of the "coagulation concentration" were obtained by this operation; this term has been used because observations using the ultra-microscope and the electron microscope indicated the occurrence of coagulation at concentrations above this critical value. It has already been shown in Part 3 how the coagulation concentration of the surface active agent salts is intimately related to the coagulation with corresponding cations, for a silver iodide sol protected with the surface active

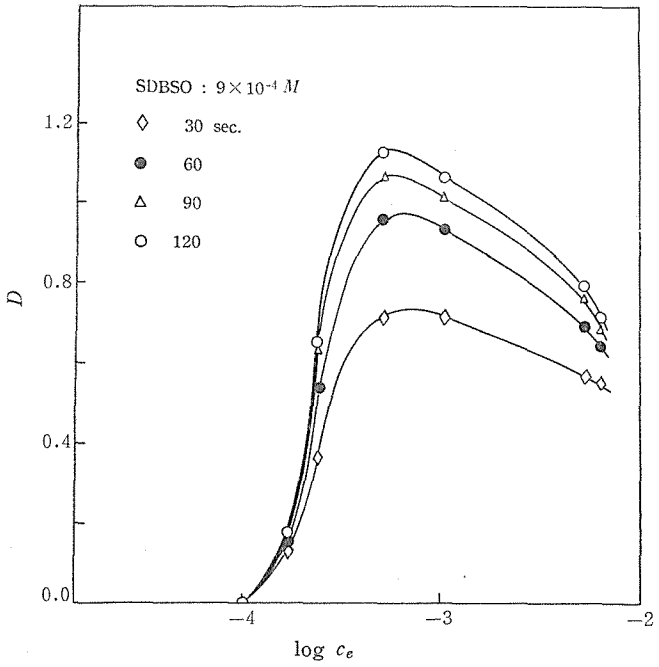

Fig. 4. Optical density *vs.* log molar concn. of $La(NO_3)_3$ for formation of lanthanum dodecyl benzenesulphonate at various times after mixing.

agent.

The values of the coagulation concentration obtained by the above procedure are given in Table 2, see later.

In Fig. 5, 6 and 7 the optical densities (90 sec after mixing) are plotted against the logarithm of the electrolyte concentration for the reactions between various cations and TS^-, $DBSO^-$ and DP^- ions, respectively.

It can be seen that in the formation of thorium salts well-defined peaks are observed at certain concentration ranges of the electrolyte; the lanthanum salts, however, show much broader humps. These are intimately related to the mobility behaviour of the sol particles formed, see later.

In the case of salts of the divalent cations, the optical density usually increases with the cation concentration in the high concentration range. Although the increase in supersaturation must be taken into account in explaining this behaviour, coagulation of the sol formed is also taking place in this region, see Discussion.

Anomalous behaviour is observed for the reactions between manganese and DP^- and between barium or calcium and TS^- ions. These systems show well defined peaks at lower concentrations in addition to the main peaks, see Fig. 5 and 6. Hence two values of coagulation concentration are given in Table 2, corresponding to these two sets of peaks. It was observed that floccule formation was taking place in the coagulation range at lower concentration; this gave rise to a marked inhomogeneity of the sol formed. As the electrolyte concentration was increased, the floccules were transformed into large clusters of particles and the sol became optically homogeneous. Here, "floccule" is taken to mean a very bulky and less-

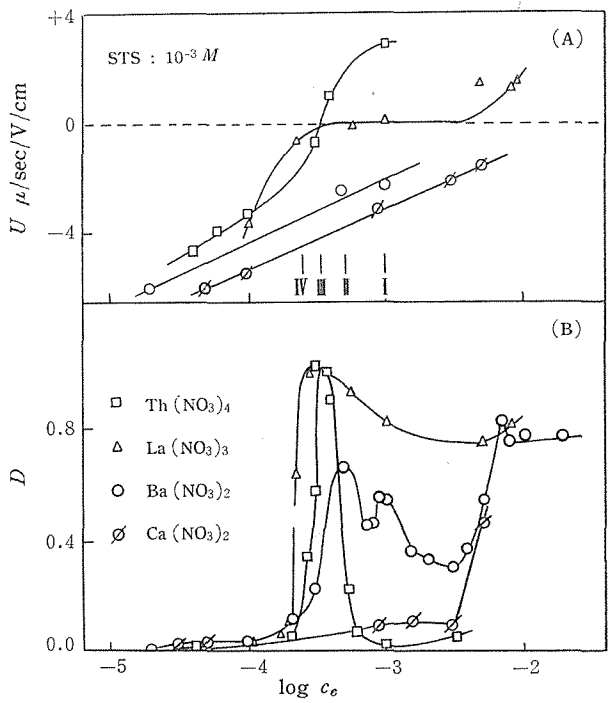

Fig. 5. Formation of tetradecyl sulphate salts.

(A) Electrophoretic mobility *vs.* log molor concn. of added electrolytes.
(B) Optical density, 90 sec. after mixing, *vs.* log molar concn. of added electrolytes.
I, II, III, IV : Equivalent concns. of uni-, di-, tri-, and tetravalent cations.

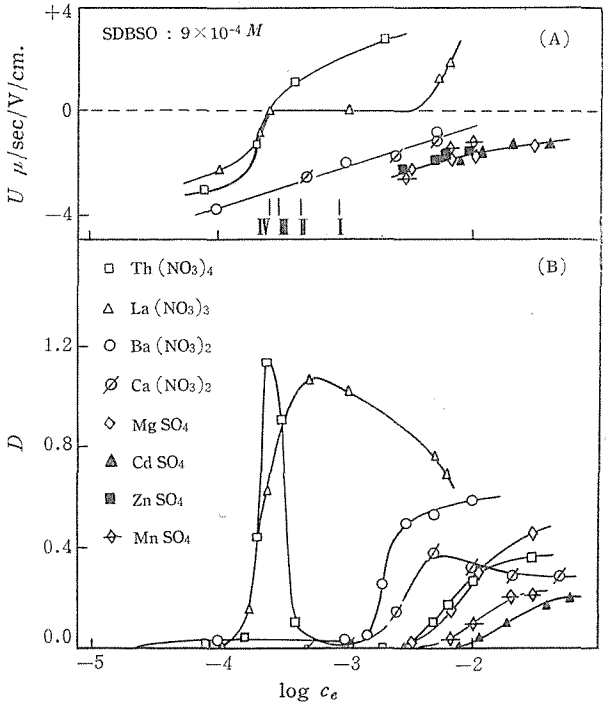

Fig. 6. Formation of dodecyl benzenesulphonate salts.

(A) Electrophoretic mobility *vs.* log molar concn. of added electrolytes.
(B) Optical density, 90 sec. after mixing, *vs.* log molar concn. of added electrolytes.
I, II, III, IV : Equivalent concns. of uni-, di-, tri- and tetravalent cations.

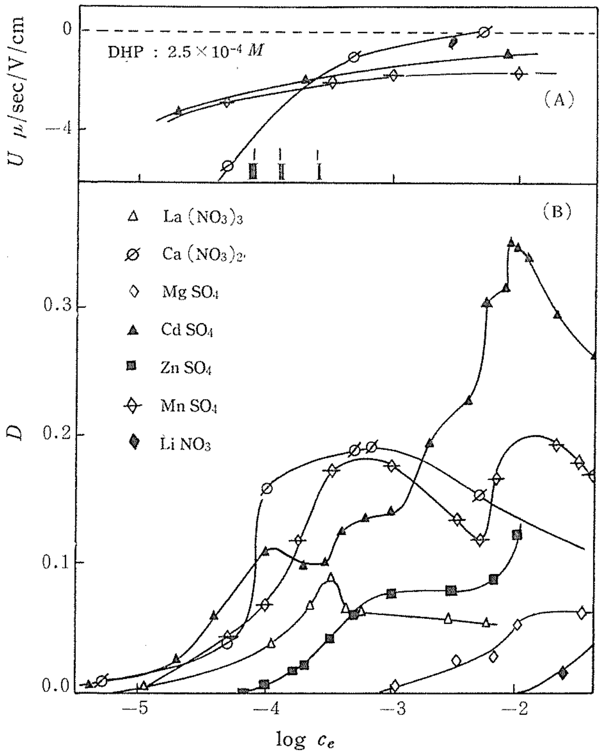

Fig. 7. Formation of dodecyl phosphate salts.

(A) Electrophoretic mobility *vs.* log molar concn. of added electrolytes.
(B) Optical density, 90 sec. after mixing, *vs.* log molar concn. of added electrolytes.
I, II, III : Equivalent concns. of uni-, di- and trivalent cations.

tightly bound coarse collection of particles, and "cluster" to mean a very tightly bound dense collection of particles.

In the case of the $Ba(TS)_2$ sol, the peak at lower concentration is again subdivided into two peaks. However, this may be due to the optical inhomogeneity of the sol formed in the cell.

(iii) Solubility

The solubility products of the metal salts of the surface active anions have been derived from the lowest concentrations of cations at which the turbidity changes were observed. The values given in Table 1 were calculated by substituting the experimental data in the following equation :-

$$\text{Solubility product} = [M^{v+}][SAA^-]^v$$

where M^{v+} and SAA^- are the v-valent metal ion and the surface active anion, respectively. For example, the solubility product of $La(TS)_3$, 4.0×10^{-14}, was obtained by substituting in this equation the experimental value of this lowest concentration of the lanthanum ion, $4.0\times10^{-2}\,M$, and the concentration of TS^- ion in the initial solution in the cell, $10^{-4}\,M$.

If complete dissociation of the salt of the surface active agent is assumed, *viz.*

$$\underset{x}{M\,(SAA)_v} \rightleftarrows \underset{x}{M^{v+}} + v\,\underset{vx}{(SAA^-)}$$

Table 1 Solubilities and solubility products of metal salts of surface active anions

Anion	TS^-		$DBSO^-$		DP^-	
Cation	Solubility product	Solubility M/litre	Solubility product	Solubility M/litre	Solubility product	Solubility M/litre
Th^{++++}	2.0×10^{-17}	1.50×10^{-4}	3.8×10^{-17}	2.03×10^{-4}	s	
La^{+++}	4.0×10^{-14}	1.96×10^{-4}	7.3×10^{-14}	2.28×10^{-4}	1.3×10^{-16}	4.70×10^{-5}
Ba^{++}	2.0×10^{-11}	1.71×10^{-4}	8.9×10^{-12}	1.31×10^{-4}	s	
Ca^{++}	5.0×10^{-11}	2.32×10^{-4}	2.5×10^{-10}	3.98×10^{-4}	1.1×10^{-13}	3.00×10^{-5}
Mg^{++}	s**		2.6×10^{-9}	8.65×10^{-4}	5.9×10^{-11}	2.45×10^{-4}
Zn^{++}	s		2.3×10^{-9}	8.30×10^{-4}	4.1×10^{-11}	2.18×10^{-4}
Mn^{++}	s		2.9×10^{-9}	9.00×10^{-4}	1.3×10^{-11}	1.48×10^{-4}
UO_2^{++}	s		s		s	
Cd^{++}	s		5.1×10^{-9}	1.08×10^{-4}	9.4×10^{-14}	2.86×10^{-5}
Li^+	s		s		3.8×10^{-6}	1.93×10^{-3}

** s ; soluble

the solubility of the salt can be calculated using the following equation :-

$$v^v.\ x^{1+v} = \text{solubility product}$$

where x is the solubility in moles per litre. The values of solubility thus obtained are listed in Table 1.

Very few values have been reported of the solubility of this kind of salt. According to Reid and Tartar[4] the solubilities of the calcium salts of dodecyl (DS^-) and cetyl (CS^-) sulphates are 110 and 5 mg per litre at 250°C, respectively. The value obtained in the present experiments for $Ca(TS)_2$ is 1.84×10^{-4} mole per litre or 62.7 mg per litre, which gives a reasonable intermediate value between the above values for C_{12} and C_{16} salts.

According to Dean and Ambrose[5], the relative solubilities of various metal salts of DS and CS give the following cationic series in increasing solubility, *viz.*

DS ; insoluble salts Al, Ba, Ce, Cr, Fe, Pb, Sr, Th, Sn, Zr
soluble salts Sb, Bi, Cd, Ca, Co, Cu, Mg, Mn, Hg, Mo, Ni, W, V, Zn
CS ; Ba, Sr<Pb<Fe, Ca<Ag, Cu<Mg, Zn

The solubilities obtained in the present experiments give the following series :-

TS ; Th<Ba<La<Ca<Mg, *etc.* (soluble salts)

If we compare this with the above series, we find, with the exception of the thorium salt, a good agreement between the two sets of results.

2. Electrophoretic Mobility

In order to see whether the coagulation was due to changes in surface charge or only due to changes in ionic strength, electrophoretic mobilities were determined on the sol particles formed. Contrary to the case of silver iodide sols, the particles had various crystal shapes, *e. g.* needles, thin plates, *etc.* (see section 3) of varying sizes. Hence, the mobility value itself has been used to discuss the problem, since it is difficult to correct for the shape and size factors in calculating ζ potentials

from the mobility data; to some extent therefore these results are only semiquantitative.

In Fig. 5, 6 and 7 the mobilities are plotted against the logarithm of the molar concentration of the added electrolyte. Generally, the mobilities are negative even if equivalent concentrations are exceeded, except in the cases of high valent cations. This can probably be explained by the strong surface activity of the anionic species, the head groups of the latter being exposed to the solution phase and giving rise to a negative charge on the particle surface.

In the case of salts of the tetra-valent thorium ion, reversal of charge occurs very near to the equivalent concentration. The deviation of the zero point of charge from the equivalent point gives an approximate estimation of the difference in surface activity of the cationic and anionic species. The curves show that the TS^- ion is more active than the $DBSO^-$ ion and the latter ion has nearly the same activity as that of thorium ion.

Reversal of charge also occurs in the case of lanthanum salts, although it does not occur in the case of lanthanum ion binding to the silver iodide sol particles protected with STS, see Part 3. The effect is less marked than in the case of the thorium ion and reversal occurs at cation concentrations much higher than the equivalent concentration. It is interesting to notice that in this case the mobility remains zero over a comparatively wide concentration range before it assumes positive values; in the case of the thorium ion the mobility *vs.* log c_e curve crosses the zero charge line obliquely. In other words, we can define a zero "point" of charge in the latter case, but only a zero "region" of charge in the former. The extensions of this region are almost the same for both TS and DBSO salts.

The mobility of $Ca(DP)_2$ approaches the value of zero at a cation concentration of 5×10^{-3} *M*. The different shape of the mobility *vs.* log c_e curve from that obtained with other divalent ions clearly shows the occurrence of cation binding. In this connexion it is found that, in general, barium and calcium ions exhibit stronger binding than other divalent cations. However, the binding takes place to a lesser degree than with the tri- and tetra-valent ions, *i. e.* lanthanum and thorium ions. In this sense barium and calcium ions lie between the trivalent and the ordinary divalent cations.

The other divalent ions apparently show almost no binding to the surface, and the decrease in mobility at higher cation concentrations can probably be explained almost entirely by the increase in ionic strength.

3. Electron Micrographs

In Fig. 8 the electron micrographs of some surface active agent salts are given.

The set of micrographs (A) are for $Ba(TS)_2$. (A_1), (A_2) and (A_3) are the salts obtained at barium concentrations of 10^{-4} *M*, which is in the concentration range of small turbidity change with time, see Fig. 5. Typical hexagonal crystals can be found. They are thin flat plates with a stepped structure. (A_4) and (A_5) are for barium concentrations of 5×10^{-4} *M*, which is in the concentration range of large turbidity change with time, see Fig. 5. In this case, long rod shaped crystals can be observed among the hexagonal crystals of more or less the same size as in

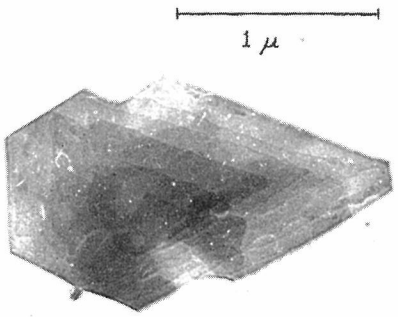

(A_1) $Ba(TS)_2$
$[Ba^{++}] = 10^{-4}\,M$
$[TS^-] = 10^{-3}\,M$

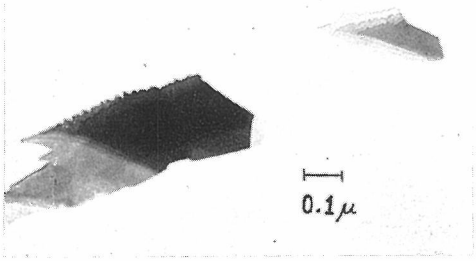

(A_2) $Ba(TS)_2$
$[Ba^{++}] = 10^{-4}\,M$
$[TS^-] = 10^{-3}\,M$

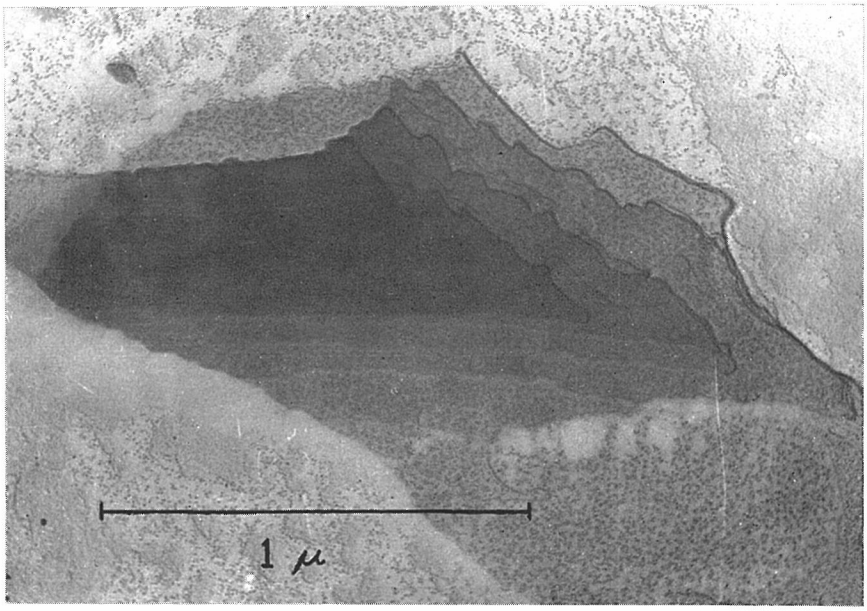

(A_3) $Ba(TS)_2$
$[Ba^{++}] = 10^{-4}\,M$
$[TS^-] = 10^{-3}\,M$

Fig. 8. Electron micrographs of metal salts of anionic surface active agents.

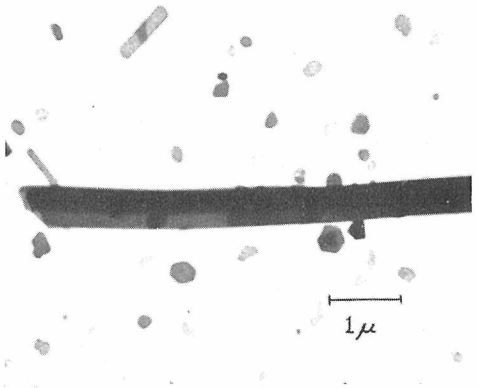

(A_4) $Ba(TS)_2$
$[Ba^{++}]=5\times10^{-4}M$
$[TS^-]=10^{-3}M$

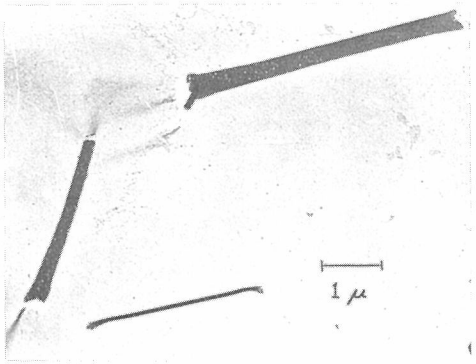

(A_5) $Ba(TS)_2$
$[Ba^{++}]=5\times10^{-4}M$
$[TS^-]=10^{-3}M$

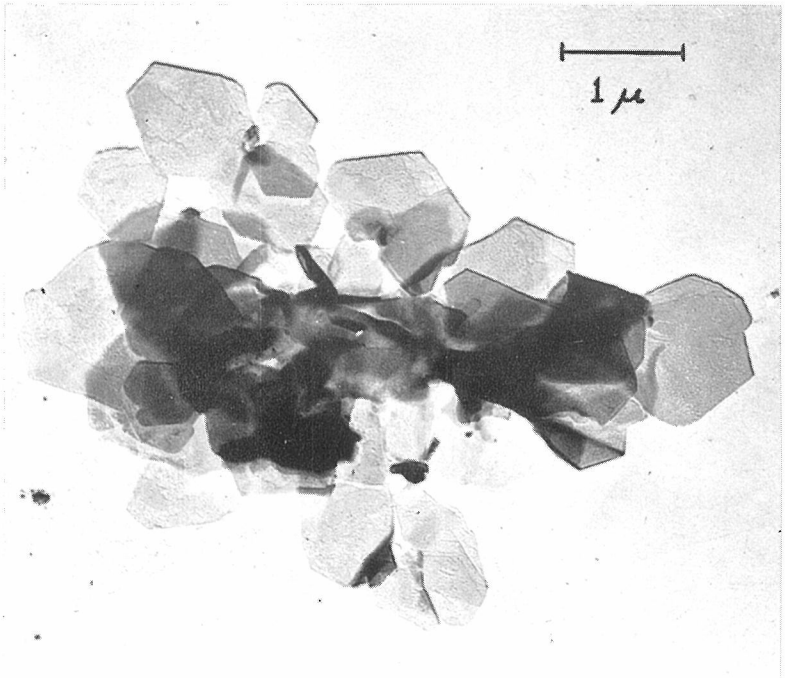

(B_1) $Cd(DP)_2$
$[Cd^{++}]=2\times10^{-4}M$
$[DP^-]=2.5\times10^{-4}M$
10 sec after mixing

Fig. 8. Electron micrographs of metal salts of anionic surface active agents.

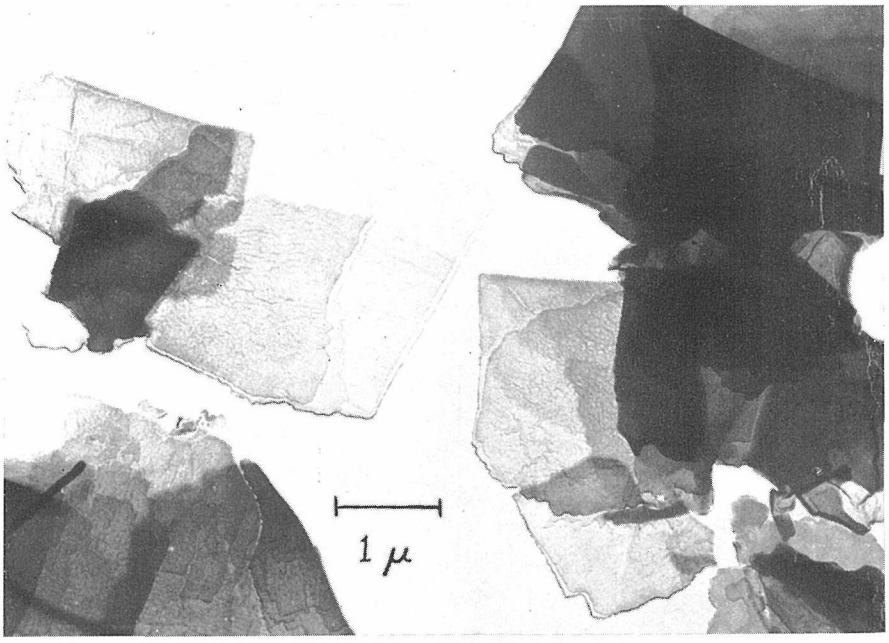

(B_3) $Cd(DP)_2$
$[Cd^{++}] = 2\times10^{-4}\,M$
$[DP^{-}] = 2.5\times10^{-4}\,M$
100 sec after mixing

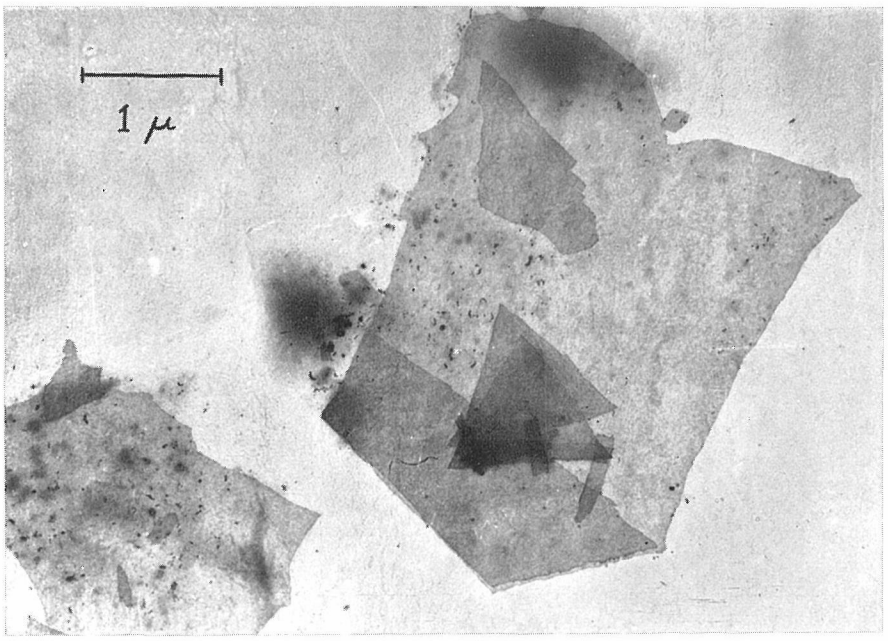

(C) $La(DBSO)_3$
$[La^{+++}] = 2.07\times10^{-4}\,M$
$[DBSO^{-}] = 9\times10^{-4}\,M$

Fig. 8. Electron micrographs of metal salts of anionic surface active agents.

(A_1), (A_2) and (A_3). It is supposed that the hexagonal crystals grow in the direction of the stepped face to a long needle.

The set of micrographs (B) are for $Cd(DP)_2$ at the cadmium concentration of 2×10^{-4} *M*. (B_1) was taken at 10 sec after mixing the electrolyte with the DHP solution, see Fig. 3. These show how coagulation of thin crystal plates is taking place; after 10 sec small aggregates of large square thin plates are observed and after 100 sec large aggregates of hexagonal thin plates can be found.

The micrograph (C) is for $La(DBSO)_3$ at the lanthanum concentration of 2.07×10^{-4} *M*, which is in the concentration range of large turbidity change, see Fig. 6. Very thin plates can be observed.

IV. DISCUSSION

1. Solubility

In order to examine the general aspects of interactions between cations and surface active anions, so called cation solubility spectra have been constructed for salts of TS^-, $DBSO^-$ and DP^- ions. These are shown in Fig. 9.

The solubility of a salt depends primarily on the valencies, radii and polarisabilities of the cationic and anionic components. Higher valency increases the electrostatic binding strength, whilst the larger polarisability strengthens the covalent bond. However, the effect of the ionic radius is complicated, since the larger ionic radius decreases the Coulombic force but increases the polarisability.

If the cationic species of the same group are compared in these cation solubility spectra, various sequences can be found. As we can expect a lower solubility for

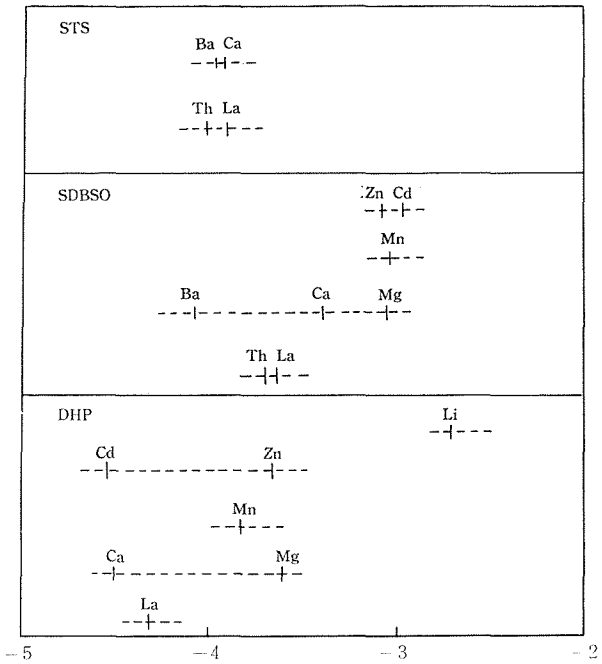

Fig. 9. Cation solubility spectra.

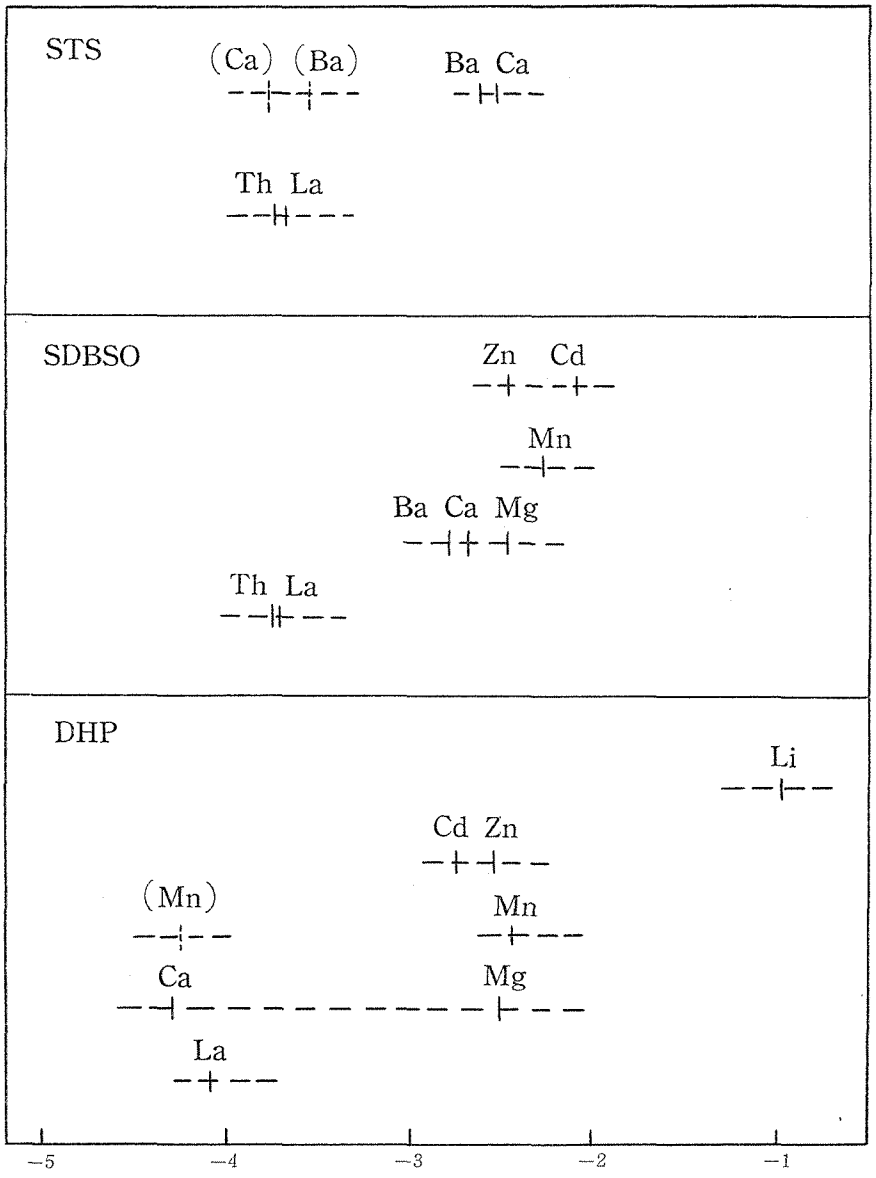

Fig. 10. Cation coagulation spectra for various surface active agent salts. The elements bracketed thus, (Ca), (Ba), (Mn), refer to initial floccule formation.

stronger interaction between the cationic and anionic species, we obtain from the spectra the following cationic sequences for ascending bond strengths:

for TS salts, Mg<Ca<Ba
for DBSO salts, Cd<Zn and Mg<Ca<Ba
fof DP salts, Zn<Cd and Mg<Ca

On the other hand, we have the following sequences for ascending cationic radii[12]:

$Mg < Ca < Ba$ and $Zn < Cd$.

From a comparison of these sequences, it can be concluded that, for ions of the alkaline earth metals, bonds between the cations and the surface active anions are primarily covalent, because the bond strength is stronger for the larger cation. The same situation holds for bonds between zinc or cadmium and DP^- ions. On the other hand, the bonds of these ions with $DBSO^-$ ions appear to be primarily electrostatic in nature; the sequence is inverted in this case.

2. Coagulation Behaviour

(i) Coagulation Concentration

The values of the coagulation concentration for various cations [see section III, 1, (ii)] are given in Table 2.

Table 2 Coagulation concentrations for sols of surface active salts

Anion Electrolyte	TS^- (10^{-3} *M*) *M*	$DBSO^-$ (9×10^{-4} *M*) *M*	DP^- (2.5×10^{-4} *M*) *M*
$Th(NO_3)_4$	1.9×10^{-4}	1.8×10^{-4}	s
$La(NO_3)_3$	2.1×10^{-4}	1.9×10^{-4}	8.3×10^{-5}
$Ba(NO_3)_2$	2.8×10^{-4} a 2.4×10^{-3} b	1.6×10^{-3}	
$Ca(NO_3)_2$	1.7×10^{-4} a 2.9×10^{-3} b	2.0×10^{-3}	5.3×10^{-5}
$MgSO_4$	s	3.3×10^{-3}	
$ZnSO_4$	s	$3,3\times10^{-3}$	
$MnSO_4$	s	5.0×10^{-3}	5.5×10^{-5} a 4.5×10^{-3} b
$UO_2(NO_3)_2$	s	s	s
$CdSO_4$	s	8.0×10^{-3}	1.8×10^{-3}
$LiNO_3$	s	s	1.0×10^{-1}

a Concentration for floccule formation
b Concentration for cluster formation
s Soluble

It is very useful to compare them with the theoretical values to be expected from the Schulze-Hardy rule[19]. According to this rule, the ratio of the coagulation concentrations of uni-, di-, tri- and tetravalent ions is as $1 : (1/2)^6 : (1/3)^6 : (1/4)^6$, *i.e.* $1 : 1.6\times10^{-2} : 1.4\times10^{-4} : 2.4\times10^{-5}$. If we assume the coagulation concentration of univalent cations to be 10^{-1} *M* (the value of the lithium ion as given in Table 2), then most of the values given in the table for divalent ions are of the right order of magnitude; in the cases of $Ba(TS)_2$, $Ca(TS)_2$ and $Mn(DP)_2$, we must use the concentration of cluster formation instead of that of floccule formation, in order to obtain agreement. It can be concluded therefore that in these cases coagulation is caused primarily by a change in ionic strength rather than a change in surface charge.

It must be remembered, however, that even if the surface potential is not

lowered sufficiently to produce coagulation and ionic strength plays the predominant part in the coagulation process, the Schulze-Hardy rule cannot be expected to hold rigorously. That is, the rule will hold only in the case of changing ionic strength for sol particles with the same surface charge density[13], *e. g.* for a silver iodide sol at the same value of *p*Ag. As the particle charges are different for different sols of surface active agent salts and also for different cation concentrations, this rule gives only approximate orders of magnitude for the coagulation concentrations. Moreover, some of the ionic species are consumed in forming the insoluble sol particles and do not contribute to the ionic strength of the medium; this gives another cause for deviation from ideality. Thus, the solubility of the salt formed has an influence on coagulation which is in the opposite sense to the relation between solubility and binding strength; this is clearly shown by the comparatively high value of the coagulation concentration for $Cd(DBSO)_2$, a salt which has a high solubility, see Table 1.

This leads at the same time to the conclusion that the particle charges will have the same value if the solubility and coagulation concentration are the same. This condition is nearly fulfilled by $Ba(TS)_2$ and $Ca(TS)_2$, by $Mg(DBSO)_2$, $Zn(DBSO)_2$ and $Mn(DBSO)_2$, and also by $Mg(DP)_2$ and $Mn(DP)_2$, *cf.* Tables 1 and 2. Hence, it can be anticipated that the binding energies between the cations and the corresponding surface active anions will be similar, within each group of sols.

(ii) Optical Density and Mobility

It is clear from Fig. 5 and 6 that the peaks of the optical density *vs.* log c_e curves coincide exactly with the zero points of charge for both $Th(TS)_4$ and $Th(DBSO)_4$. This supports the idea that coagulation takes place due to a change in the surface charge in the case of high valent cations. In fact, a stabilized finely dispersed sol was observed at concentrations higher than the zero point of charge, and cluster formation in the concentration range near the zero point of charge.

In the coagulation of lanthanum salts both charge and ionic strength change. The coagulation concentrations are of the order of magnitude expected from the Schulze-Hardy rule, see last section, and therefore it must be concluded that ionic strength is playing an important part. Since reversal of charge was actually observed in these cases, the potential must also change.

It is interesting to notice that the initial peaks in the optical density *vs.* log c_e curves for barium and calcium salts occur at concentrations corresponding to fairly high values of mobility (floccule formation). Moreover, at these concentrations the ionic strengths are not high enough to produce coagulation. This suggests that coagulation is not due either to changes in ionic strength or to changes in surface charge. One possible explanation of this phenomenon is cationic bridge formation between the univalent surface active anions of two particles. Although this effect will also be specific, it will probably give a very weak particle binding; that is, the number of bridges between the particles will be comparatively small for steric reasons. The high negative electrophoretic mobility at this concentration shows that neutralisation of the surface charge by bridge formation is still far from complete. The coagula are therefore loosely bound; this is confirmed by ultramicroscopic and optical density observation, see previously.

(iii) Cation Coagulation Spectra

The effect of the cation in coagulation becomes clearer if the cation coagulation spectra are constructed, see Fig. 10.

These spectra show marked similarities to the cation solubility spectra in Fig. 9. The cationic sequences in each group are exactly the same for both sets of spectra, if sols containing the same surface active anion are compared. This strongly suggests that the binding between the cation and the surface active anion is the same in nature for solubility and for adsorption. This concept was also found to be true for silver iodide sols protected with STS, see Part 3.

On the other hand, the relative position of each cationic group in the spectra is shifted towards a higher concentration range in the case of (Ba, Ca) for TS salts, (Zn, Cd), (Mn) and (Ba, Ca, Mg) for DBSO salts, and (Li), (Cd, Zn), (Mn) and (Mg) for DP salts, as compared with their position in the solubility spectra. This can be explained by the effect of ionic strength described in the last section. That is, the positions of these cations in the coagulation spectra are all in the range between 10^{-3} to 10^{-2} M and the position of the univalent lithium ion is in the range of 10^{-1} M, as expected from the Schulze-Hardy rule.

However, the fact that the same sequences hold for each group as those of solubility means that cationic specificities play a part in defining the fine structures of the spectra. In other words, although the order of magnitude of the coagulation concentration is determined mainly by the ionic strength, small differences in the surface charge also occur due to cation binding on the particle surface.

The position of the calcium ion for the DP salt remains at about the same concentration in both coagulation and solubility spectra, whereas for other ions, *e. g.* Mg^{++}, a large shift occurs. This behaviour can also probably be explained by bridge formation in the case of calcium DP salts.

The positions of the thorium and lanthanum ions are always very near to those in the solubility spectra.

3. Reaction Mechanism of the Whole Process

Since the turbidity does not follow the Rayleigh relation, see Part 2, in the case of non-spherical particles once they have become greater than a certain size[9] and as in the present case very asymmetric particles were obtained, we shall restrict ourselves to a qualitative discussion of the turbidity changes with time.

(i) General Considerations

The mechanism of the reaction which takes place after addition of the electrolyte to the surface active agent solution is complicated. It would appear that the process takes place in several steps, *viz.* nucleation[14], crystal growth[14] and coagulation (or sensitisation)[15], these steps occurring consecutively or simultaneously, according to conditions. Although the surface active agent concentrations were kept constant, the concentration of the cation was changed from less than equivalent to considerably greater than equivalent. The reaction rate of each step is, in general, influenced by the absolute concentration of reactants, by the surface charge of the particles formed and by ionic strength; the last two factors are again functions of

the relative and absolute amounts of cationic and anionic species of the system.

The optical density *vs.* time curves obtained in the experiments (see Fig. 1, 2 and 3) can be classified into eight types of curves which are illustrated in Fig. 11. (A) and (B) are the types of curve usually obtained in sol formation, *i. e.* no coagulation taking place. However, the curves from (C) to (H) represent superposition of sol formation and coagulation.

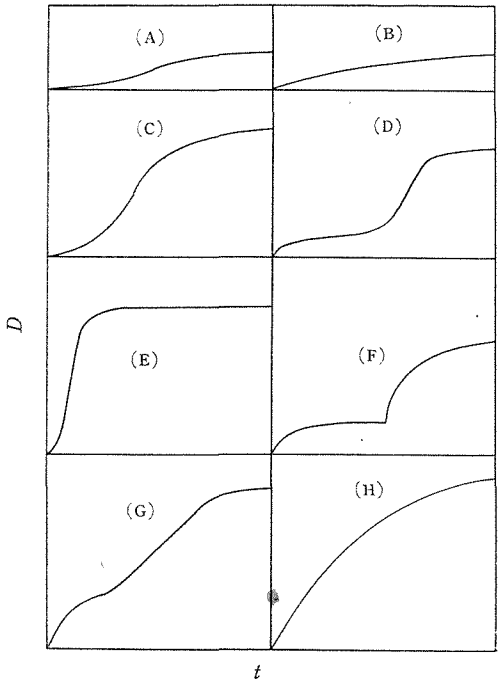

Fig. 11. Schematic diagrams showing various types of optical density *vs.* time curves for formation of insoluble salts of surface active agents.

Before discussing the conditions which give rise to these different types of curves, we shall discuss the effect of the initial condition on each step.

(ii) Nucleation

a. Rate of Nucleation. The nucleation stage involves the formation of clusters consisting of a few surface active salt molecules. The clusters with sizes larger than a critical value are called "nuclei" and tend to grow to larger particles, however, those with smaller sizes tend to dissociate into ions. The critical size can be derived from the thermodynamic consideration of the two phases, *i. e.* solution and solid[16,17,18]. The local free energy change, ΔF_i, is related to the number of molecules in the cluster, i, by the expression

$$\Delta F_i/kT = A_1 i^{2/3} - A_2 i \qquad (1)$$

where A_1 is a constant proportional to the interfacial free energy per unit area of the two phases and A_2 is a constant proportional to the bulk free energy difference between them. Hence, $\Delta F_i/kT$ has a maximum value, $\Delta F_n/kT$, when $i=n$, where

$$\Delta F_n = 4 A_1^3/27 A_2^2 \qquad (2)$$

and

$$n = 2 A_1/3 A_2 \qquad (2A)$$

This value, n, gives the critical size of the clusters, *i. e.* nuclei.

The rate constant of nucleation, k_n nuclei per mole per sec, has been related to the free energy, ΔF_n, by the use of fluctuation theory[16,17], as

$$k_n = K_1 \exp\left[-(\Delta F_n + W_n)/kT\right] \qquad (3)$$

where W_n is the energy of activation for diffusion across the phase boundary and K_1 a constant[17]. Various attempts have been made to evaluate K_1, but this problem will not be discussed here.

In the formation of sols of surface active salts investigated in the present work, the cation concentration was changed while the surface active anion concentration was kept constant. Hence, the net nucleation rate is obtained by multiplying k_n by the cation concentration. This means that the nucleation rate increases linearly with cation concentration. Therefore, the number of nuclei, and hence the number of sol particles, increases with the cation concentration. However, since nucleation is followed by crystal growth, this number does not increase indefinitely with cation concentration, and its upper limit is defined by the relative speeds of these two steps. If the value of ΔF_n or W_n is very large and hence the nucleation takes place very slowly followed by rapid crystal growth, the number of particles increases with cation concentration, until the nucleation rate becomes much larger than the crystal growth rate, while, if the opposite situation occurs, the number of particles becomes practically constant at fairly low cation concentrations, because the nucleation rate is sufficiently high at this concentration.

Both cases have been observed. For instance, in the formation of $Cd(DP)_2$, the number of particles was much larger at higher cation concentrations, but the particle size remained virtually constant over the concentration range, in which the nucleation rate effected the whole reaction mechanism. On the other hand, in the formation of $Zn(DBSO)_2$, the particle size was much larger at higher concentrations, but the particle numbers were practically constant, except in the very low cation concentration range.

b. Induction time. Another quantity which must be mentioned in connexion with the nucleation process is the "induction time", T_i[14]. This is the period of time which passes after mixing the two reactants before a pronounced turbidity change can be observed. This has been related to the initial concentration. c_e, by an empirical equation, *viz.*

$$T_i = K_2 c_e^{-m} \qquad (4)$$

where K_2 and m are constants which are different for different systems, *e. g.* $m = 5$, 4, 7, 9 and 3.3 for AgCl, Ag_2CrO_4, CaF_2 and Ca-oxalate[19]. In the case where the reactants are not equivalent, *e. g.* the present case, c_e must be replaced by the geometric mean ionic concentration, $\bar{c}_e$, *e. g.* $\bar{c}_e = ([Ag^+][I^-])^{1/2}$ for AgI, $([Cd^{++}][TS^-]^2)^{1/3}$ for $Cd(TS)_2$, *etc*[19].

It is clear from equation (4) that if K_2 is small a fairly large induction time

can be expected at low cation concentrations. This is the reason why a sigmoid type of curve is very often observed even if no coagulation is taking place, see the curve (A) in Fig. 11. The values of K_2 and m vary for the different reactions studied; for very small K_2 and large m, T_i is practically zero and no induction time will be observed, see curve (B) in Fig. 11.

(iii) Crystal Crowth

The growth of nuclei will almost certainly be influenced by the surface charge of the particles. Mobility measurements showed that the negative surface charge of the particles decreased with increasing cation concentrations in the case of high valent cations and alkaline earth ions. Hence, the increase in cation concentration enhances the rate of crystal growth in two ways, *i. e.* by decreasing the surface charge and by increasing the supersaturation of the initial solution.

a. General equation of crystal growth. The growth of a particle with mass m and surface area S is expressed by the following equation[19,20],

$$dm/dt = k^{\delta} S (c_i - c_i^s) \qquad (5)$$

where

$$k^{\delta} = k_f \exp(-\Delta F^{\neq}/kT) \qquad (5A)$$

Here k^{δ} is the interfacial reaction rate constant, k_f the frequency factor of the interfacial reaction, $\Delta F^{\neq}$ the free energy of activation, and c_i and c_i^s are respectively the surface concentration and saturation concentration of the cation or anion. If the ionic deposition on crystal surfaces is a reversible process and there is no potential barrier to inhibit the surface reaction, $\Delta F^{\neq}$ corresponds to the free energy of activation of diffusion; this is the case at the zero point of charge. However, if the surface charge retards one of the surface reactions, *i. e.* cationic deposition or anionic deposition, this becomes the rate-determining step of the whole crystal growth process, and therefore c_i and c_i^s in equation (5) must be taken as the corresponding concentrations of either cation or anion, depending on which is the slow reaction.

b. The effect of surface charge on supersaturation. It is well known that the solubility of a small particle is larger than that of a large particle. Moreover the dependence of solubility on the particle radius is influenced by the surface charge density[21] because of the extra interfacial free energy due to the electrical double layer. However, calculation has shown that this influence is small compared with the intrinsic solubility of the particle, see Appendix. Hence, we can assume that c_i^s in equation (5) is not influenced significantly by the change in surface charge density.

c. The effect of surface charge on $\Delta F^{\neq}$. This effect can be discussed, by analogy to electrode kinetics[22,23], by drawing the potential energy diagram of the depositing ionic species, see Fig. 12. For the sake of simplicity the retarding effect of positive charge on cationic deposition will be discussed; the effect of negative charge on anionic deposition can be discussed in the same way, if the sign is reversed.

Curve I shows the potential energy curve for an unsolvated cation in the external layer of the crystal lattice, with coordinate x_1. Curve II is the potential

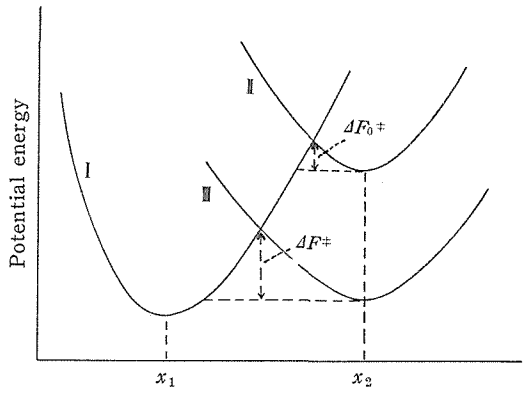

Fig. 12. Potential diagram of a depositing ion on a particle surface.

energy curve for a solvated ion at the outer Helmholtz plane, x_2, when the surface is uncharged. Hence, the free energy of deposition is given by $\Delta F_0^{\neq}$; in the case of the growth of ionic crystals, it is unnecessary for the depositing ion to be discharged, and hence the potential barrier between these two layers will probably be the only potential barrier to be considered for a surface reaction mechanism. If the particle surface has a positive charge, an extra potential difference arises, and the curve II will therefore be shifted downwards to curve III by an amount $ve(\psi_2 - \psi_1)$, where v is the valency of the cation. As the value of ψ_2 equals zero for curve II, the net decrease in the potential energy is $ve\psi_2$ ($\cong ve\zeta$). Hence, the free energy of activation for a charged surface, $\Delta F^{\neq}$, is given by

$$\Delta F^{\neq} = \Delta F_0^{\neq} + \alpha ve\psi_2 \qquad (6)$$

where α is a proportionality factor determined by the slope of curve I, and $0<\alpha<1$ (transfer coefficient).

This gives a possible explanation of the retardation of the particle growth. That is, the surface charge of a particle enhances the activation energy for the deposition of the ionic species having a charge of the same sign and this reaction becomes the rate-determining step of the whole crystal growth process. This mechanism corresponds to "activation polarisation" in electrode processes. However, it must be remembered that in some cases the deposition process is reversible without any potential barrier. In this case the reaction rate constant is not influenced by the change in surface charge.

The above mechanism of retardation may be occurring in the formation of lanthanum and thorium salts of surface active anions, where reversal of charge occurs, and also in the formation of barium and calcium salts, where the surface charge is decreasing with increasing cation concentration.

However, for other ions the particle charge remains practically constant and the increase in crystal growth rate is only due to increase in reactant concentration, *i. e.* supersaturation.

d. The effect of surface charge on surface concentration. In equation (5) $k^{\prime}$ is not the net reaction rate constant but the heterogeneous *surface* reaction rate

constant. Hence, the concentration to be used for c_i is not the bulk concentration, c_{ib}, but the interfacial concentration. The latter is related to the former by the Boltzmann equation, *viz.*

$$c_i = c_{ib} \exp(-z_i e \psi_2 / kT) \qquad (7)$$

That is, the cation surface concentration is lowered by the presence of a positive surface charge, which can also retard the crystal growth. This corresponds to "concentration polarisation".

e. General shape of the crystal growth curve. It is not at all easy to solve equation (5) and relate it to the optical density *vs.* time curves. However an attempt will be made in Part 6 for the early stages of crystal growth when the supersaturation is very high. At the low concentrations, in which we are mainly interested in this paper, the term $(c_i - c_i^s)$ in equation (5) is small and we cannot neglect the decrease in c_i with time.

Qualitatively, the rate of crystal growth becomes very small in a much shorter period of time at low concentrations than it does at high concentrations. Therefore, the particle volume *vs.* time curve, and hence the optical density *vs.* time curve, tends to a limiting value more rapidly.

(iv) Coagulation

This process is due either to reduction of surface charge or to increase in ionic strength, and can be treated in exactly the same manner as in the last three papers. The optical density *vs.* time curve has a linear form in the initial stages but after a time the rate of increase of optical density decreases.

(v) The Overall Reaction

This can be treated by combining each of the steps discussed in the foregoing sections.

Curves (A) and (B) are combinations of nucleation and crystal growth. These curves are observed at very low supersaturations, low ionic strengths and high particle charges. It was confirmed by electron microscopy that no coagulation was taking place in this case; the optical density increase was very small compared with other types of curves. Type (A) is found when the nucleation step has an induction time and (B) is found when the nucleation is rapid and has no induction time.

Type (C) has been observed in reactions where a curve of type (A) was found at lower concentrations, *e. g.* $Mn(DP)_2$, see Fig. 2. Hence, this suggests a combination of sol formation of type (A) followed by coagulation of the sol.

If the concentration is further increased, the curve assumes the form of either type (E) or (D) depending on whether the induction time of nucleation is still observable or not at this concentration, *e. g.* $Mn(DP)_2$ or $Cd(DP)_2$. It can be assumed that crystal growth still continues to take place after coagulation starts.

Type (F) is a typical consecutive reaction, *viz.* crystal growth and coagulation; the latter process starts to take place after all of the ionic species have been consumed in crystal growth. The fact that the first stage of the curve corresponds to crystal growth and the second to coagulation has been confirmed by electron mi-

croscopy.

It is interesting to compare the two types of curves in the formation of $Cd(DP)_2$, *e. g.* the curves for 1×10^{-4} and 2×10^{-4} *M* Cd^{++}, see Fig. 3. Although the concentration is higher for the latter curve, which is of type (F), the optical density is smaller than for the former curve, which is of type (D), at least until *ca.* 120 sec after mixing. This can be explained in the following manner. For conditions leading to curves of type (D), crystal growth will not be complete and unreacted ionic material will be remaining in the solution. Therefore more ions will be deposited on the larger particles, which have coagulated, than on to the smaller particles; this follows because the deposition reaction is heterogeneous and the rate is proportional to surface area; *cf.* equation (5). In the case of type (F), even though the rate of crystal growth per unit area is larger due to the higher concentration, the coagulation starts only after the crystal growth of the primary particles has become almost complete; hence no ionic material remains in solution. The coagulation, therefore, takes place only between these primary particles. This kind of competition between the two mechanisms can contribute to the optical density change only in a very narrow concentration range; if the concentration is sufficiently high, the optical density change is always larger at higher concentrations.

Type (G) is observed at high concentrations, *e. g.* with $Cd(DP)_2$ at concentrations higher than 2×10^{-3} *M*. This type of curve can be explained as a combination of very rapid initial crystal growth followed by coagulation.

Type (H) is exactly the same as that to be discussed in Part 6 and can be considered as the simultaneous occurrence of crystal growth and coagulation. A typical example of this type of curve is found in the formation of $Ba(TS)_2$, see Fig. 1.

The author wishes to express his gratitude to Dr. R. H. Ottewill, the University of Cambridge, for his kind supervision during the course of this work, to the British Council for the award of the Scholarship and to the University of Cambridge for the Oliver Gatty Studentship. Thanks are also due to Dr. R. W. Horne, Cavendish Laboratory, for taking electron micrographs, and to Imperial Chemical Industries, Dyestuffs Division, for supplying the STS, late Dr. A. V. Few for the SDBSO, and to Dr. H. C. Parreira for the DHP. The author's thanks are also due to Professor I. Tachi and to Dr. S. Ueda for their continuous interest and encouragement.

APPENDIX

THE EFFECT OF SURFACE CHARGE ON THE SOLUBILITY OF A PARTICLE

It is well known that the solubility of small particles differs from that of large particles, the functional relationship between the solubility, *S*, and the particle radius, *a*, being given by

$$S = S_\infty \exp(2\gamma M/a R T d) \qquad \text{(A. 1)}$$

where *M* and *d* are the molecular weight and density of the particle, γ the interfa-

cial tension and S_∞ the solubility of a large mass, *i. e.* $S \to S_\infty$ for $a \to \infty$. The effect of surface charge on this relationship was derived by Knapp[21] on the basis of the Helmholtz model of the double layer. However, as this model does not give an appropriate picture of the interface, see Part 4, an extension of this theory has been made by the use of the Gouy model of the double layer.

The total free energy of the interface, F, can be expressed formally as the sum of an ordinary interfacial free energy, F_γ, and electrical free energy, F_{el}, *viz.*

$$F = F_\gamma + F_{el} \tag{A. 2}$$

where $$F_\gamma = 4\pi a^2 \gamma \tag{A. 3}$$

and

$$F_{el} = -(\varepsilon a/2)(1+\kappa a)\psi_\delta^2 \tag{A. 4}^{8,9}$$

Substitution of equations (A. 3) and (A. 4) in equation (A. 2) gives

$$F = \left(4\pi\gamma - \frac{\varepsilon\kappa\psi_\delta^2}{2}\right)a^2 - \frac{\varepsilon\psi_\delta^2}{2}a \tag{A. 5}$$

As the mass of the particle, is given by

$$m = (4/3)\pi a^3 d$$

and hence

$$dm = 4\pi a^2 d \cdot da$$

we obtain

$$dF = \frac{1}{d}\left[\left(2\gamma - \frac{\varepsilon\kappa\psi_\delta^2}{4\pi}\right)\frac{1}{a} - \frac{\varepsilon\psi_\delta^2}{8\pi}\frac{1}{a^2}\right]dm$$

Considering an infinitesimal process of transferring a mass dm from a particle of radius a_1 to another of radius a_2, we obtain, by integration, the following equation, *viz.*

$$\frac{RTd}{M}\ln\frac{S_1}{S_2} = \left(2\gamma - \frac{\varepsilon\kappa\psi_\delta^2}{4\pi}\right)\left(\frac{1}{a_1} - \frac{1}{a_2}\right) - \frac{\varepsilon\psi_\delta^2}{8\pi}\left(\frac{1}{a_1^2} - \frac{1}{a_2^2}\right)$$

where $S = S_1$ for $a = a_1$

and $S = S_2$ for $a = a_2$.

By taking $S_2 \to S_\infty$ for $a_2 \to \infty$, we obtain

$$S = S_\infty \exp\left[\left\{\left(2\gamma - \frac{\varepsilon\kappa\psi_\delta^2}{4\pi}\right)\frac{1}{a} - \frac{\varepsilon\psi_\delta^2}{8\pi}\cdot\frac{1}{a^2}\right\}\frac{M}{RTd}\right] \tag{A. 6}$$

$$= S_\infty \exp\left[\left\{\frac{2\gamma}{a} - \frac{\varepsilon\psi_\delta^2}{8\pi a^2}(2\tau+1)\right\}\frac{M}{RTd}\right] \tag{A. 7}$$

This is the relation between the solubility and the surface potential of a particle. On comparing equations (A. 7) and (A. 1), it is found that the solubility of a particle is decreased by the presence of a surface charge.

The value of S as a function of a has a maximum value, S_{max}, at $a = a_{max}$, where

$$S_{max} = S_\infty \exp\left[\frac{(8\pi\gamma - \varepsilon\kappa\psi_\delta^2)^2}{8\pi\varepsilon\psi_\delta^2}\cdot\frac{M}{RTd}\right] \tag{A. 8}$$

and $$a_{max} = \varepsilon\psi_\delta^2/(8\pi\gamma - \varepsilon\kappa\psi_\delta^2) \tag{A. 9}$$

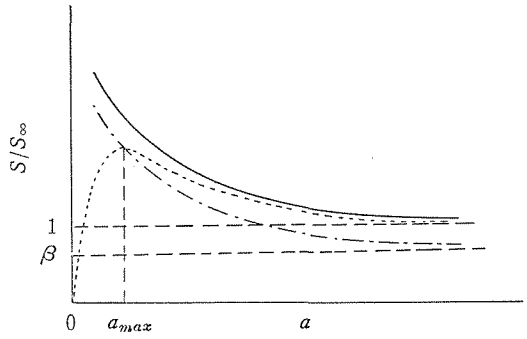

Fig. A. 1. Theoretical solubility *vs.* radius curve for a small particle.

——— Absence of surface charge
..... Corrected for diffuse double layer
..... Corrected for constant surface charge density

In Fig. A. 1 the general shape of the curve given by this relation is illustrated.

In the case of silver iodide sols, however, the effect of surface charge on solubility is very small. For example, if we take $\gamma=400$ ergs/cm^2, $\psi_\delta=0.1$ volt, $a=10^{-6}$cm and $\kappa a=1.23$, we obtain

$$F_\gamma \cong 5.04\times10^{-9} \text{ erg}$$

and $$F_{el} \cong 10^{-11} \text{ esu.}$$

Hence, the surface charge has practically no influence on the total interfacial free energy, *i. e.* $F_\gamma \gg F_{el}$. In equation (A. 7), the second term of the exponential term becomes about 10% of the first term for the value of a smaller than 2 Å, and the value of a_{max} is less than 1 Å. These values of a are improbable in the system of major interest.

The above discussion may, however, be an under-estimation, since the Gouy theory is not sufficient to describe the whole picture of the double layer, see Part 4. Therefore, the total surface charge density, $\sigma=\sigma_1+\sigma_2$, must be used instead of σ_2. If we assume that the total surface charge of a particle, q, is proportional to the surface area, we obtain

$$F_\gamma=4\pi\gamma a^2 \quad \text{and} \quad F_{el}=q^2/\varepsilon a=16\pi^2 a^3\sigma^2/\varepsilon$$

By the same method as before, the following equation can be obtained:-

$$S=\beta S_\infty \exp(2\gamma M/RT\, ad) \qquad \text{(A. 10)}$$

where $$\beta=\exp(-12\pi\sigma^2 M/RT\,\varepsilon\, d) \qquad \text{(A. 11)}$$

In Fig. A. 1 the general shape of the curve given by this relation is illustrated.

However, substitution of the experimental value of σ, *i. e. ca.* 3 μcoul/cm^2 for a sol of pAg 3 as extrapolated from Mackor's data[24], shows that under these conditions the correction factor β is not significant.

It is important to point out here that the equation derived by Knapp is based on a rather unreasonable assumption; this is, that the total charge of a particle remains constant irrespective of the change in particle radius. Although this treatment leads to an expression for the solubility as a function of the particle radius,

which has a maximum at certain value of a, this equation reduces to an equation similar to equation (A. 10) and gives no maximum, if we make the more reasonable assumption, that q is proportional to the surface area. Therefore, discussions based on this aspect of his theory would not seem to be correct.

REFERENCES

(1) A. Watanabe, This Bulletin, 38, 216 (1960).
(2) B. Težak, E. Matijević, K. F. Schulz, J. Kratohvil, M. Mirnik and V. B. Vouk, *Disc. Faraday Soc.*, 18, 63 (1954).
(3) B. Težak, E. Matijević and K. F. Schulz, *J. Phys. and Colloid Chem.*, 55, 1557, 1567 (1951).
(4) R. M. Reed and H. V. Tartar, *J. Am. Chem. Soc.*, 58, 322 (1936).
(5) R. S. Dean and P. M. Ambrose, *U. S. Bur. Mins. Bull.*, 449 (1944).
(6) A. M. Gaudin, "Flotation," McGraw Hill, New York (1957).
(7) K. L. Sutherland and I. W. Wark, "Principles of Flotation," Australian Institute of Mining and Metallurgy, Melbourne (1955).
(8) A. Watanabe, This Bulletin, 38, 179 (1960).
(9) H. A. Abramson, "Electrokinetic Phenomena", Chem. Catalog, New York (1940).
(10) H. C. Parreira, Ph.D. Thesis, Cambridge (1958).
(11) A. Watanabe, This Bulletin, 38, 274 (1960).
(12) L. Pauling, "The Nature of the Chemical Bond", 2nd ed., Cornell Univ. Press, New York (1940).
(13) E. J. Verwey and J. Th. G. Overbeek, "Theory of Stability of Hydrophobic Colloids", Elsevier, Amsterdam (1948).
(14) W. E. Garner, "Chemistry of the Solid State", Butterworths, London (1955).
(15) A. Watanabe, This Bulletin, 38, 158 (1960).
(16) R. Becker and W. Döring, *Ann. Physik*, (5), 24, 719 (1935).
(17) D. Turnbull and J. C. Fischer, *J. Chem. Phys.*, 17, 71 (1949).
(18) M. Volmer, "Kinetik der Phasenbildung", Dresden (1939).
(19) A. E. Nielsen, *J. Colloid Sci.*, 10, 576 (1955).
(20) R. A. Johnson and J. D. O'Rourke, *J. Am. Chem. Soc.*, 73, 380 (1951).
(21) L. F. Knapp, *Trans. Faraday Soc.*, 17, 457 (1922).
(22) R. Parsons, in Bockris', "Modern Aspects of Electrochemistry", 1. Butterworths, London (1954).
(23) R. Audubert, *Disc. Faraday Soc.*, 1, 72 (1947).
(24) E. L. Mackor, *Rec. trav. chim.*, 70, 763 (1951).